Computer simulation and six-dimensional spin density and velocity NMR microimaging of lacunar systems: A comparative analysis of percolation properties

H.-P. Müller, J. Weis, and R. Kimmich

Universität Ulm, Sektion Kernresonanzspektroskopie, 89069 Ulm, Germany

(Received 6 June 1994; revised manuscript received 25 April 1995)

Using computer-simulated random site-percolation networks as a template, phantoms of lacunar systems were fabricated. The pore space was filled with water and experimentally investigated with the aid of nuclear magnetic resonance (NMR) microimaging. A pulse sequence providing six-dimensional spin density and velocity NMR image data was employed for the combined record of the three-dimensional spin density distribution and the three-dimensional velocity vector field of water percolating through the pore networks. From these data, three-dimensional velocity magnitude images were derived. The exclusion of all voxels of the spin density images with velocities below the noise level provides an experimental means to directly image the percolation backbone. An evaluation procedure for the NMR image data was established that reliably renders the pair correlation function and the mean volume-averaged porosity as a function of the probe volume radius. Characteristic parameters refer to the fractal dimensionality, to the correlation length, and to the short-range order. The theoretical predictions can thus be compared directly with experiment. For comparison, the water-filled pore spaces of other, less random lacunar objects such as glass-bead agglomerates and a natural sponge were also examined with respect to percolation properties.

PACS number(s): 47.55.Mh, 87.59.Pw, 47.53.+n, 61.43.Hv

I. INTRODUCTION

Fractals and random percolation clusters can be well characterized by parameters such as the fractal dimension and the correlation length [1, 2]. Corresponding power laws have been predicted and verified by computer simulations in the two-dimensional case [3–5].

Percolation clusters are also of interest with respect to transport processes [6]. However, in this case the backbone of the percolation cluster is relevant, rather than the percolation cluster itself. In a finite percolation cluster, the backbone is usually defined as the set of pathways conducting an electrical dc current between two points, or sets of points, kept at different potentials [7]. As a subset of the percolation cluster, the backbone is formed by removing all dangling ends, branches, etc., that do not contribute to the conductivity [8]. A typical situation, where the percolation backbone acts as the transport-limiting structure, is flow of fluids through porous media.

Random percolation networks form fractal structures within the correlation length [2]. In this study we are referring to a more extended class of systems, which may be termed "lacunar." This includes ideal fractals and percolation clusters rigorously complying to the definitions, but also materials such as natural sponges or glass-bead agglomerates. The structure of such porous media cannot be considered to be self-similar in general, of course. However, depending on the degree of disorder, there is a tendency towards an analogous behavior: It will be shown, for instance, that the mean volume-averaged porosity as a function of the probe volume radius below the correlation length often fairly well obeys a power law. An objective of this work is to elucidate the applicability

limits of the characterization of lacunar systems on this basis.

In this study we compare computer-simulated data and experimental data obtained with the aid of nuclear magnetic resonance (NMR) microscopy [9]. Lacunar objects can be easily modeled on a computer. The properties of the simulated percolation objects can be opposed to those of real lacunar systems. The samples may be of natural origin or can be fabricated artificially using computer simulation data as a "template."

Solid matrix materials normally do not contribute to the signals recorded in spin-echo imaging experiments with liquidlike samples. Therefore the liquid-filled pore space of the lacunar samples can directly be imaged with the aid of NMR microscopy methods. These techniques permit us to record the three-dimensional distribution of the liquid as well as the three-dimensional field of the flow velocity. On the basis of such imaging data sets, any two- or three-dimensional representation of the local spin density or the local velocity can be rendered. The local spin density is equivalent to the local porosity of the material, where "local" refers to the voxel at the considered position. Spin density images mirror the full percolation cluster, whereas the percolation backbone can be visualized based on the velocity data.

The simulated and the measured data can be evaluated in the same way. This in particular means that the same statistical procedures can be applied. Thus direct juxtapositions become feasible.

NMR microimaging has already been employed for the experimental record of three-dimensional distributions of matter in porous media [10–13]. The lower limit of the accessible length scale is a matter of detection sensitivity.

With objects about 1 cm in diameter, the sensitivity-limited voxel resolution is about $50 \times 50 \times 50 \ \mu m^3$.

The upper limit is given either by the field of view or by the diameter of the samples fitting into the probehead (and this into the magnet bore). At least two orders of magnitude of length can be covered with one experimental setup. The range can be extended part by part in supplementary experiments with smaller or larger samples of the same sort using probeheads adapted to the sample size.

II. DEFINITIONS

The porosity is defined by

$$\rho = \frac{V_p}{V_p + V_m},$$ (1)

where V_p is the total pore volume and V_m is the total matrix volume without pores in the sample fraction under consideration. We distinguish the "overall porosity" referring to the whole sample and the "local porosity" characterizing the situation within a voxel at a certain position.

In the NMR imaging experiments described in the following the pores were filled with water. The local porosity $\rho = \rho(r_i)$ is then equal to the local spin density, that is, the volume fraction of the water in the voxel under consideration. Therefore, the water signal amplitude arising from this voxel is directly proportional to the local porosity.

The proportionality factor is $K = S_0/(N\bar{\rho}_0)$, where S_0 is the total signal amplitude, N is the total number of voxels, and $\bar{\rho}_0$ is the average porosity of the whole sample. $\bar{\rho}_0$ can be determined from the weights of the dry matrix material (m_m) and the fluid-filled sample $(m_w + m_m)$ according to

$$\bar{\rho}_0 = \frac{m_w}{m_w + q \, m_m},$$ (2)

where q is the ratio of the mass densities of the fluid and the matrix material.

A function of particular interest in this context is the dependence

$$\bar{\rho}_V(r) = \frac{1}{N_p} \sum_{i=1}^{N_p} \frac{1}{N_v} \sum_{j=1}^{N_v} \rho(r_j) \quad (r \le |r_i - r_j|),$$ (3)

where r is the radius of a spherical probe volume. $\rho(r_j)$ is the porosity in the voxel at the position r_j. N_v is the number of voxels in the probe volume. For evaluations below the correlation length of the cluster, the center of the probe volume must be at a position r_i belonging to the considered cluster. The condition $r \le |r_i - r_j|$ is the consequence of the spherical shape of the probe volume. The expression in Eq. (3) finally refers to the ensemble mean value of N_p probe volumes of equal size. The quantity $\bar{\rho}_V(r)$ will be called "mean volume-averaged porosity."

The disordered structure of porous materials can be studied also by a radial distribution analysis, which is otherwise used for the characterization of the short-range order in amorphous solids, liquids, and gases [14, 15]. In this procedure, the pair correlation function $g(r)$, correlating the local porosities of voxel pairs with a fixed distance r, is of particular interest.

The average porosity of the voxels in the centers of an ensemble of N_p spherical probe volumes of equal size can be compared with the "mean surface-averaged porosity," $\bar{\rho}_A(r)$, referring to voxels on the probe-volume surfaces. $\bar{\rho}_A(r)$ is formed in the following manner. The average of the local porosities of the N_v voxels on the surface of a probe volume of radius r is taken in a first step. The result is the surface-averaged porosity $\rho_A(r)$. This quantity is formed for all possible N_p probe volumes, from which the ensemble mean value $\bar{\rho}_A(r)$ is taken.

The pair correlation function is then defined by

$$g(r) = \frac{\bar{\rho}_A(r)}{\bar{\rho}_c},$$ (4)

where

$$\bar{\rho}_c = \frac{1}{N_p} \sum_{i=1}^{N_p} \rho(r_i)$$ (5)

is the ensemble mean value of the porosities in the center voxels of the probe volumes. In more detail, the evaluation formula for the pair correlation function is

$$g(r) = \frac{1}{\bar{\rho}_c} \frac{1}{N_p} \sum_{i=1}^{N_p} \frac{1}{N_v} \sum_{j=1}^{N_v} \rho(r_j) \quad (r = |r_i - r_j|).$$ (6)

The subscripts i and j refer to the center and surface voxels of the probe volume, respectively.

III. TECHNICAL DETAILS OF THE NMR EXPERIMENTS

The proton magnetic resonance imaging experiments were carried out with a Bruker Biospec 47/40 magnet (4.7 T) equipped with a radio frequency unit composed of commercial and homemade components. The receiver, converter, modulator, and filter were units of the Bruker Biospec series. The linear transmitter was purchased from Kalmus, the preamplifier from Doty, the personal-computer-based pulse sequence and shape programmer from Surrey Medical Imaging Systems Ltd. The gradient amplifiers, the interfaces, and the tomograph operating software were homemade. The maximum gradients were 0.6 T/m. Typical gradient switching times were 0.2 ms.

Three-dimensional (proton) spin density image data were recorded using a gradient-recalled echo pulse sequence [9]. The spatial information was encoded with the aid of two phase-encoding and one frequency-encoding gradient pulses. The adjusted resolution was 0.1 or 0.25 mm in each dimension. The sample thickness was 8 mm and 16 mm, respectively.

Velocity vector fields were measured using a modification of the Fourier-encoding velocity imaging (FEVI) technique [16, 17]. The pulse scheme is shown in Fig. 1. The local velocity is encoded with the aid of bipolar gradient pulses for the velocity components in addition to the gradient pulses for spatial encoding.

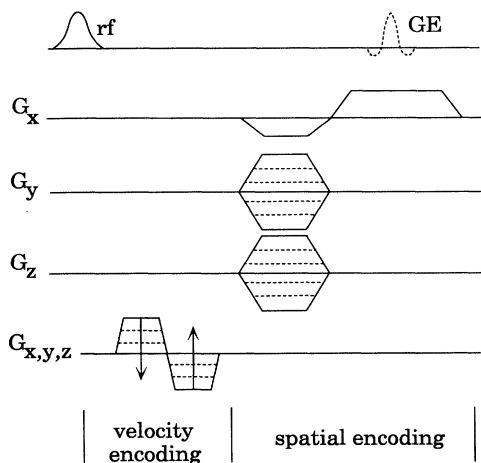Lacunar phantoms (Fig. 2) were fabricated in the

FIG. 1. Radio frequency (rf) and field gradient (G_x, G_y, G_z) pulse scheme for the record of three spatial and three velocity components. The latter are addressed in subsequent transients. The technique is called six-dimensional Fourier-encoding velocity imaging (FEVI). The spatial information is recorded by two phase-encoding and one frequency-encoding gradient pulses. For the measurement of the three components of the local velocity vector, three phase-encoding, i.e., bipolar, gradient pulses are subsequently employed. The signal is acquired as a gradient-recalled echo (GE).

form of stacks of 0.5-mm-thick polystyrene disks. The pores in the disks were machined according to computer-generated templates. For this purpose, a computer-controlled plotter-based milling machine (Leiterplatten Kopierfräsen GmbH) was employed. The pore networks were based on a cubic lattice. The extension of the relevant sample structure was 32 lattice constants in each space direction. The cross section of the pores was rectangular with an edge length of 0.5 mm.
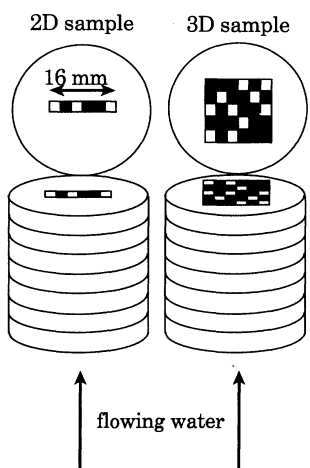

FIG. 2. Schematic illustration of the fabrication of two- (2D) or three-dimensional (3D) models of lacunar systems. The models were composed of 32 polystyrene disks of a thickness of 0.5 mm. The pore textures in the disks were machined according to computer-simulated templates. The cross section of the pores was rectangular with an edge length of 0.5 mm.

As an example of a lacunar system of natural origin, a water-filled sea sponge was investigated. The sponge was slightly pressed to fit tightly in a sample tube. Glass-bead agglomerates were considered as a model system with a pore structure ordered to an appreciable degree. Other systems of interest in this context may be materials encountered in oil recovery or building industries [11].

The porous samples were filled with static or flowing water so that the pore space could be imaged using the NMR methods mentioned above. Air bubbles in the pores were carefully eliminated by evacuation before water was injected.

A prerequisite for the evaluation procedure is that transverse relaxation losses can be neglected or, if not, that the transverse relaxation rate averaged over a voxel is the same at all positions in the sample. Also, there should be no inhomogeneities of the static magnet field within the field of view. This condition was tested by magnetic resonance spectroscopic imaging [18]. It turned out that the static magnet field variations were less than ± 0.15 ppm at all positions within the samples.

IV. COMPUTER SIMULATION OF TWO- AND THREE-DIMENSIONAL LACUNAR SYSTEMS

A. Random percolation clusters

The simulations were carried out assuming the same spatial resolution relative to the object size as operational in the experiments, that is, a pixel and voxel resolution of either 0.1 mm or 0.25 mm. The site-percolation clusters were composed on a cubic lattice with the aid of the random-number generator or the Borland C programming language. The occupation of two neighboring lattice sites was interpreted as a pore in between. The corresponding treatment of all lattice sites led to the desired percolation network [see Fig. 3(a), for instance]. In view of the intended use of the computer-simulated patterns as templates for the fabrication of phantoms, only matrix patterns without "islands" were considered.

The resulting pore network was then examined with respect to statistical parameters and the extension of the percolation clusters. The mean volume-averaged porosity $\bar{\rho}_V(r)$ was determined as a function of the radius r of the probe volume by the aid of Eq. (3).

In most computer simulations previously reported in literature [3, 7], the mean volume-averaged porosity $\bar{\rho}_V(r)$ in a spherical probe volume, the center of which is on an occupied lattice point in the middle of the largest cluster, was calculated as a function of the radius. The probe-volume radii are varied in integer steps, until the edge of the lattice matrix is reached [see Fig. 4(a)]. According to the available computer time, a number in the order of 1000 independent percolation networks is generated with the same netpoint occupation probability p. The results are then averaged for each probe-volume radius.

This procedure works with computer simulations, but

is not feasible in real experiments. The number of independent samples that can be prepared and investigated in an experiment is restricted and does not permit averages over a sufficiently large ensemble. Therefore the so-called "sandbox" method [1] was employed, which yields equivalent evaluation accuracies. The method is illustrated and described in Fig. 4(b).

The mean volume-averaged porosity $\bar{\rho}_V(r)$ was evaluated in probe volumes with centres located at all possible positions (occupied lattice points) and for all possible radii within the sample. Then the averages over all probe volumes having the same radius were formed. It turned out that the standard deviation of these averages is reasonably low as long as the radii are much smaller than the sample dimension. Unfortunately, the probe-volume ensemble decreases with increasing radius, so that the statistical error becomes more and more unfavorable.

On the other hand, the parameters of interest, that is, the fractal dimensionality and the correlation length, are evaluated from data obtained with small probe-volume radii. A reliability test was performed with random two- or three-dimensional site-percolation networks with

site occupation probabilities above the threshold value p_c [19]. The results of the evaluation are shown in Figs. 5(a), 5(b), 6(a), and 6(b). The initial decay is expected to follow the power law [3]

$$\bar{\rho}_V \propto r^{d_f - d_E}, \tag{7}$$

where d_f is the fractal and d_E the Euclidean dimensionality.

The fractal behavior Eq. 7 is restricted to a range $a < r < \xi$, where the correlation length ξ typifies the extension of the cluster and a is the lattice constant. For $r > \xi$, the mean volume-averaged porosity approaches a constant value until it drops at the sample edges. A constant mean volume-averaged porosity indicates that the percolation cluster tends to fill the space homogeneously if regarded in a length scale far beyond the correlation length.

The matrix size, which can be examined in the three-dimensional NMR microscopy experiments, was restricted to 32 × 32 × 32. This is a matter of the available measuring time, of course. In order to test the reliability
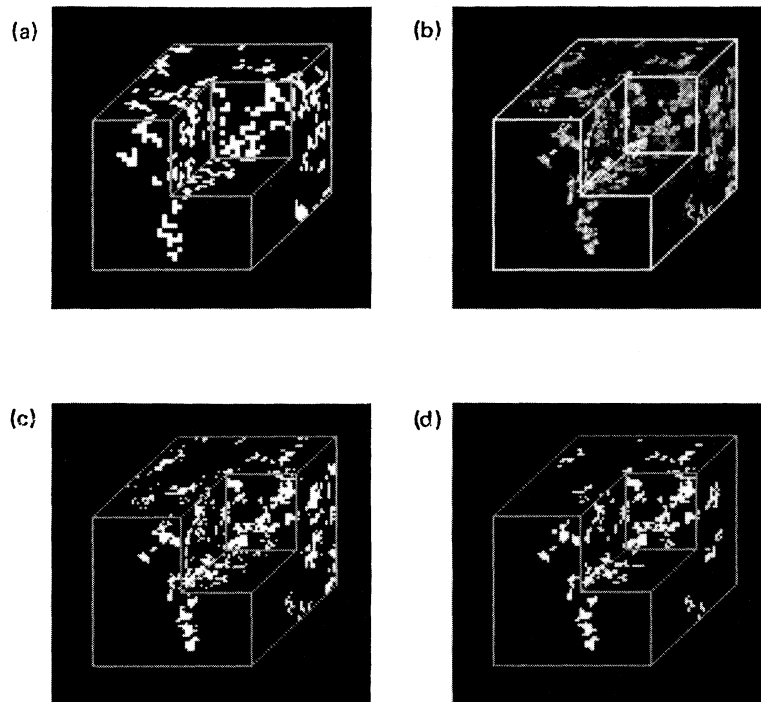

FIG. 3. Three-dimensional representations of percolation clusters. (a) Computer-simulated percolation network with a site occupation probability $p = 0.3466$, where $p_c = 0.3116$. The cubic matrix consisted of 32×32×32 lattice points. All isolated clusters were eliminated. The white voxels correspond to "pores" (displayed only if located in the planes of the shown multisectional view of the cluster). (b) Multisectional representation of three-dimensional spin density image data recorded from a water-filled percolation cluster phantom. The phantom was fabricated by taking the computer-simulated cluster (a) as a template. The voxel matrix is 64×64×64 with a resolution of 250 μm. The signal intensities of the voxels, that is, the complementary gray shades, are proportional to the average porosities in the voxels. (c) Percolation cluster evaluated from the micrograph (b) by transferring the gray shades to black-white contrasts as described in the text. (d) Percolation backbone derived from the black-white-converted spin density data (c) in combination with six-dimensional FEVI data recorded from water flowing through the phantom. The main flow direction was parallel to the vertical axis. Originally white voxels were set black if the velocity magnitude was below the noise level (0.8 mm/s) of the velocity measurements and left white otherwise.
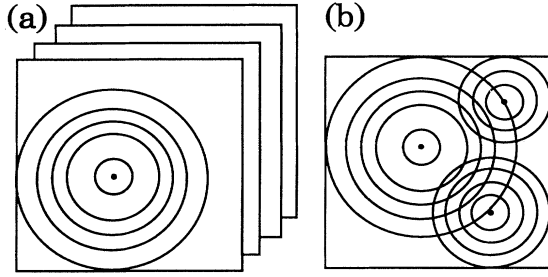
FIG. 4. Schematic (two-dimensional) illustration of the algorithms employed for the evaluation of the mean volume-averaged porosity $\bar{\rho}_V(r)$ as a function of the radius r. (a) Formation of the average over spherical probe volumes centered at fixed positions in an ensemble of independent percolation clusters. This is the standard method suitable and usual with computer simulations. (b) Formation of the average over a series of spherical probe volumes in a single percolation cluster ("sandbox" method [1]). The central points of the probe volumes are scanned over all pore voxels as far as compatible with the probe volume radius. This procedure was employed in the present study for the evaluation of the NMR micrographs as well as of the computer-simulated pore patterns, which have served as templates for the model systems.

of evaluations performed on this basis, clusters of that size were also simulated. The dependences of the correlation length and of the probability that a point belongs to the "infinite" cluster P_∞ on $p - p_c$ are plotted in Figs. 7(a) and 7(b), respectively. The expected power laws

$$\xi \propto (p - p_c)^\nu, \tag{8}$$

$$P_\infty \propto (p - p_c)^\beta \tag{9}$$

are verified in a reasonable range. The straight lines represent the theoretical dependences for exponents $\nu = -0.88$ and $\beta = 0.41$ [19]. In spite of the small size of the matrices assumed in these simulations, the results are in good agreement with the theoretical expectations, so that the same sort of evaluations can reliably be used for the experimental NMR microscopy data.

B. Bead agglomerates

A porous system frequently considered in literature [20] is an agglomerate of closely packed beads. Ideally the matrix forms a bcc structure of spheres with nearest neighbors touching each other [compare Fig. 8(a)]. The theoretical overall porosity is 0.39 according to the definition in Eq. (1). The function $\bar{\rho}_V = \bar{\rho}_V(r)$ numerically evaluated from the computer-simulated data is plotted in Fig. 9(a). The periodic structure leads to a different behavior compared with random percolation clusters, although the shapes of the $\bar{\rho}_V = \bar{\rho}_V(r)$ curves appear to be similar at first sight. The structural periodicity is reflected by an oscillatory modulation. The deviation from a power law at short radii is obvious.

The pair correlation function $g(r)$ [Fig. 10(a)] is a measure of the probability distribution of interpore distances.

By definition, $g(r)$ should approach the values 0 and 1 in the limits $r \to 0$ and $r \to \infty$, respectively. Deviations of the simulated data are due to the finite voxel and matrix sizes.
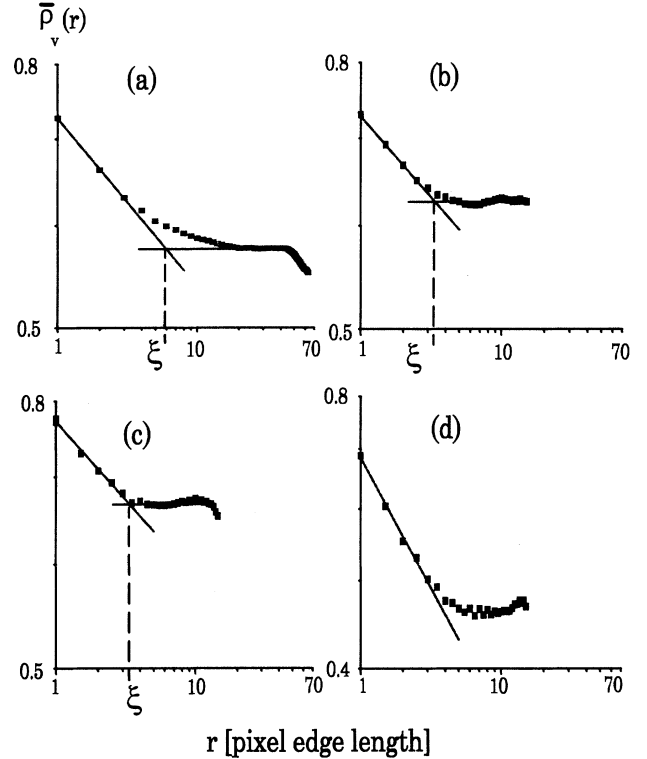

r [pixel edge length]

FIG. 5. Mean volume-averaged porosity of two-dimensional random percolation clusters versus the radius of the probe volume given in pixel edge lengths. (a) Data for a computer-simulated random percolation network with a net point occupation probability $p = 0.6377$, that is, $p - p_c = 0.045$. The cubic basis lattice consisted of 128×128 lattice points. Isolated pore clusters were eliminated. The straight lines correspond to the parameters $d_f = 1.88 \pm 0.01$ and $\xi = (6 \pm 1)$ pixel edge lengths. For comparison, the theoretical value of the fractal dimensionality is $d_f = 1.8957$ [3, 19]. (b) Data for a computer-simulated random percolation cluster with a higher netpoint occupation probability ($p = 0.6527$ and $p - p_c = 0.060$) and a matrix of 32×32 lattice points. The straight lines correspond to the parameters $d_f = 1.88 \pm 0.01$ and $\xi = (3 \pm 1)$ pixel edge lengths. (c) Experimental data evaluated from the spin density image of a water-filled, two-dimensional percolation phantom. The measured pixel matrix was 128×128 from which the central 64×64 pixels were evaluated. The pixel resolution was 250 μm. Before processing the spin density image of the (static) water, the gray shades were converted to black-white contrasts as described in the text. The phantom was machined using the computer-simulated pattern (b) as template. The straight lines correspond to the parameters $d_f = 1.88 \pm 0.01$ and $\xi = (3 \pm 1)$ pixel edge lengths. (d) Experimental data evaluated from the percolation backbone of the same phantom as in (c). The black-white-converted spin density image was velocity filtered using a velocity magnitude image recorded with the FEVI method (Fig. 1) in an experiment with flowing water. The straight line is characterized by $d_f = 1.66 \pm 0.05$.

The shape of $g(r)$ [Fig. 10(a)] again reflects the period-icity of the translational symmetry. The maxima essentially correspond to the coordination shells of a reference bead. On the other hand, submaxima that may be expected for this sort of structure are hardly resolved.

V. NMR MICROIMAGING DATA

A. Black-white evaluation of spin density images

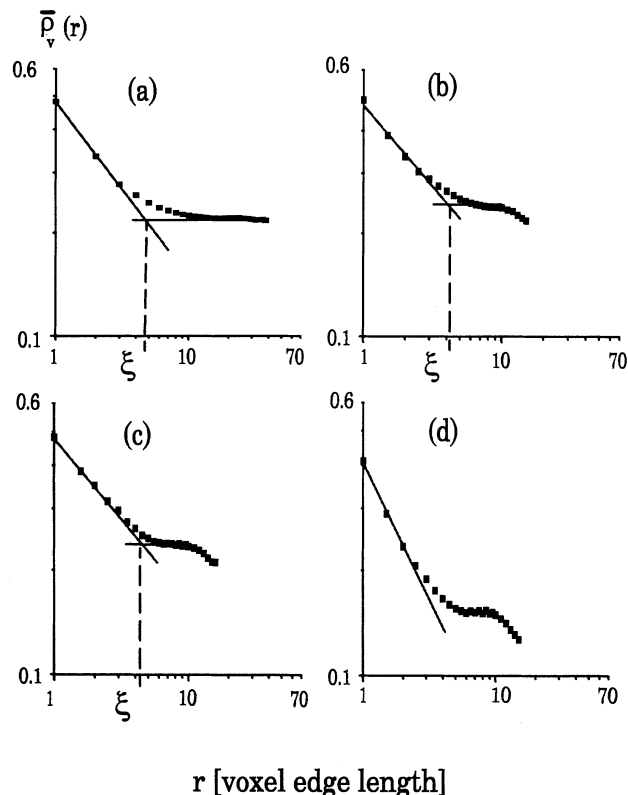The gray shades of the NMR (spin density) images such as Fig. 3(b) directly reflect the local signal intensity,

r [voxel edge length]

FIG. 6. Mean volume-averaged porosity of three-dimensional random percolation clusters (see Fig. 3) versus the radius of the probe volume measured in voxel edge lengths. (a) Data for a computer-simulated random percolation cluster (cubic lattice with $80 \times 80 \times 80$ unit cells, $p = 0.3366$, $p_c = 0.3116$ [19], and isolated pore clusters eliminated). The straight lines correspond to the parameters $d_f = 2.52 \pm 0.01$ (theoretical value 2.53 [3, 19]) and $\xi = (5 \pm 1)$ voxel edge lengths. (b) Data for a computer-simulated random percolation cluster as in (a) but restricted for $32 \times 32 \times 32$ lattice points and for a occupation probability $p = 0.3466$ [see Fig. 3(a)]. The straight lines correspond to the parameters $d_f = 2.51 \pm 0.01$ and $\xi = (4 \pm 1)$ voxel edge lengths. (c) Experimental data evaluated from a black-white-converted spin density image [Fig. 3(c)] of a water-filled phantom that was fabricated using the computer-simulated pattern Fig. 3(a) as a template. The straight lines correspond to the parameters $d_f = 2.53 \pm 0.01$ and $\xi = (4 \pm 1)$ voxel edge lengths. (d) Experimental data evaluated from percolation backbone image Fig. 3(d) [same phantom as used for (c)]. The straight line is characterized by $d_f = 2.24 \pm 0.01$.
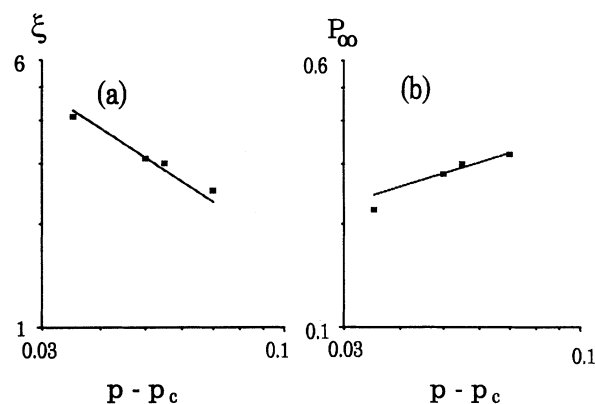

FIG. 7. Computer simulation test of the proportionalities (a) $\xi \propto (p-p_c)^\nu$ and (b) $P_\infty \propto (p-p_c)^\beta$ for three-dimensional site-percolation networks. The slopes of the straight lines represent the theoretical exponents $\nu = -0.88$ and $\beta = 0.41$.

that is, the local porosity in the voxel under consideration. In contrast to the computer-simulated clusters, the whole gray scale from black to white is represented. The intermediate gray shades arise from voxels that are only partly inside the pore space and from noise superimposed to the water signals.

The mean volume-averaged porosity [Eq. (3)] for probe volumes with radii below the correlation length is only defined for voxels belonging either to the pore space or to the matrix (as it comes out in computer simulation but not in real experiments). Therefore, for corresponding evaluations the gray shades I must be transferred to black-and-white contrasts. A straightforward procedure for this purpose is described in the following.

Referring to regions of bulk water (in large pores or outside of the matrix), the signal intensity of the voxels is first normalized by defining all voxels to be "white," which are completely filled with water, that is, the gray shade is $I = 1$. The rms noise level I_n can be determined experimentally from a region that is a priori known to be free of water, that is, from a region outside of the sample or inside a part of the matrix known to be without pores. Then the gray shade of all voxels with $I \leq I_n$ is set "black," i.e., $I = 0$. All voxels with $I \geq 1 - I_n$ are set white, that is $I = 1$.

The remaining voxels are treated in such a manner that the average gray shade $\langle I \rangle$ corresponds to the overall porosity. Let the fractions of black, white, and "intermediately" shaded voxels be f_b, f_w, and f_i, respectively, where $f_b + f_w + f_i = 1$. That is,

$$\langle I \rangle = f_i \langle I \rangle_i + f_w, \tag{10}$$

where $\langle I \rangle_i$ is the average gray shade of the intermediately shaded voxels. All voxels with $I \geq \langle I \rangle_i$ are then set white $(I = 1)$, whereas all voxels with $I < \langle I \rangle_i$ are considered to be black $(I = 0)$.
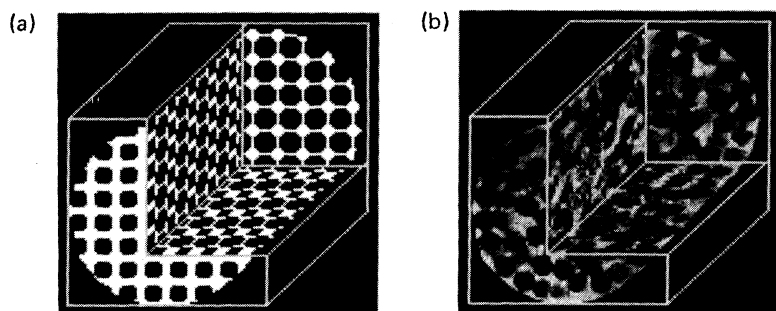
(a)   (b)

FIG. 8. Three-dimensional multisectional image representations of closely packed spheres. (a) Computer graph of an array of bcc-packed spheres. The same voxel matrix and resolution as in the experiments were assumed, that is, $80 \times 80 \times 80$ and $1/9$ bead diameters, respectively. (b) Experimental spin density image of water filled in the interstitial space of a glass-bead agglomerate. The bead diameter was (1.0 ± 0.2) mm. The voxel resolution was 100 μm.

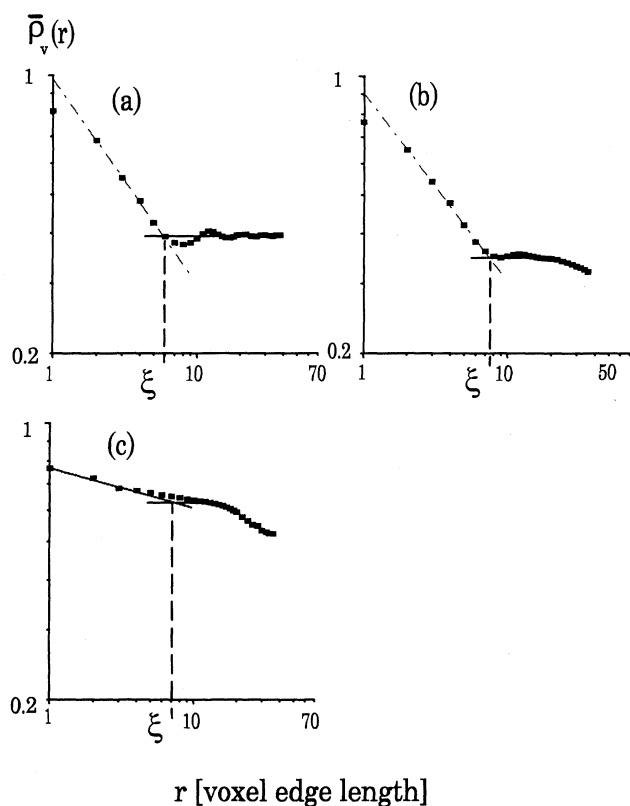$\bar{\rho}_v(r)$

r [voxel edge length]

FIG. 9. Mean volume-averaged porosities of tightly packed spheres and of natural sponge versus the radius of the probe volume measured in voxel edge lengths. (a) Data evaluated from the computer image data Fig. 8(a) for packed spheres. The decaying straight line correspond to the power law $r^{-0.52 \pm 0.02}$. The parameter ξ is (6 ± 2) voxel edge lengths. (b) Experimental data evaluated from the black-white-converted spin density image Fig. 8(b) of a water-filled glass-bead agglomerate. The decaying straight line correspond to the power law $r^{-0.48 \pm 0.02}$. The parameter ξ is (8 ± 2) voxel edge lengths. (c) Experimental data evaluated from a percolation backbone image of water-filled sponge [Fig. 12(b)]. The black-white-converted spin density image recorded in the absence of water flow was "velocity filtered" with the aid of an accompanying FEVI experiment performed with flowing water. The decaying straight lines correspond to the power law $r^{-0.09 \pm 0.01}$. The parameter ξ is (7 ± 1) voxel edge lengths.

B. Images of the percolation backbone

The combination of three-dimensional spin density images with the six-dimensional FEVI data permits the unambiguous rendering of images of the percolation backbone according to the very definition. The spin density field of the water-filled pore space was first imaged in the absence of flow. Then a parallel experiment was carried out with water percolating through the porous sample.
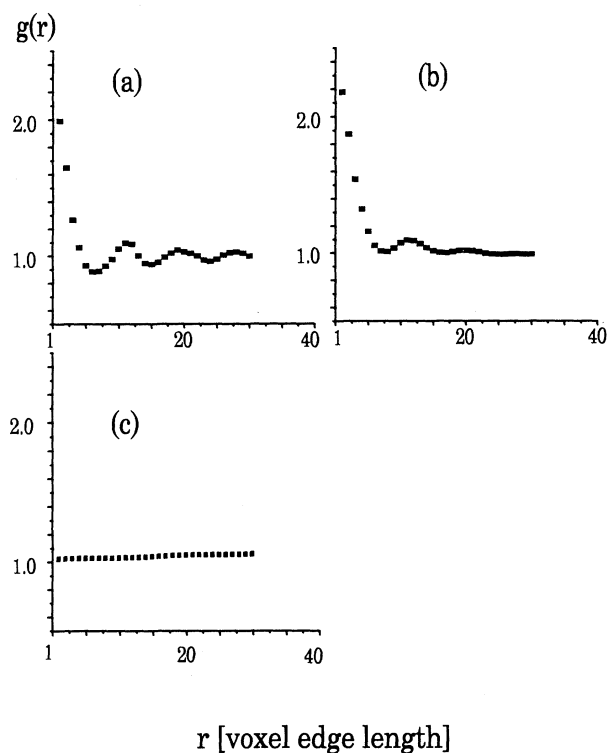
g(r)

r [voxel edge length]

FIG. 10. Pair correlation function of the pore space in different lacunar systems. (a) Data evaluated from the computer image data Fig. 8(a) of bcc-packed spheres with perfect translational symmetry. (b) Experimental data derived from the black-white-converted spin density image of static water dispersed in a glass-bead agglomerate. The image data are based on Fig. 8(b). (c) Experimental data derived from the black-white-converted and velocity-filtered spin density image of water filled in a natural sponge [Fig. 12(b)].

The goal was to suppress signals of static water, which may exist in "dead ends" of the pore space. Only voxels containing flowing water were taken into account.

In principle, the spin density information is implied in the six-dimensional FEVI data set. However, such images recorded with flowing water tend to be subject to artifacts with respect to the spin density. Therefore it appeared to be more favorable to record the three-dimensional spin density data separately in the absence of flow and use the velocity image data merely for "dead-end voxel filtering."

For each voxel, the magnitude $v = \sqrt{v_x^2 + v_y^2 + v_z^2}$ was calculated from the three velocity components determined in the FEVI experiment. The histograms of the components and the absolute values of the velocity vectors are shown in Fig. 11. The distribution demonstrates that the velocity vector field is rather "randomized" by the pore network.

The velocity magnitude image data were then combined with the black-white spin density image data described in Sec. V A. Voxels containing static water, that is, water having a velocity below the rms noise level of 0.8 mm/s, are excluded and taken as black. Voxels with higher velocities are considered to belong to the percolation backbone and are left white.
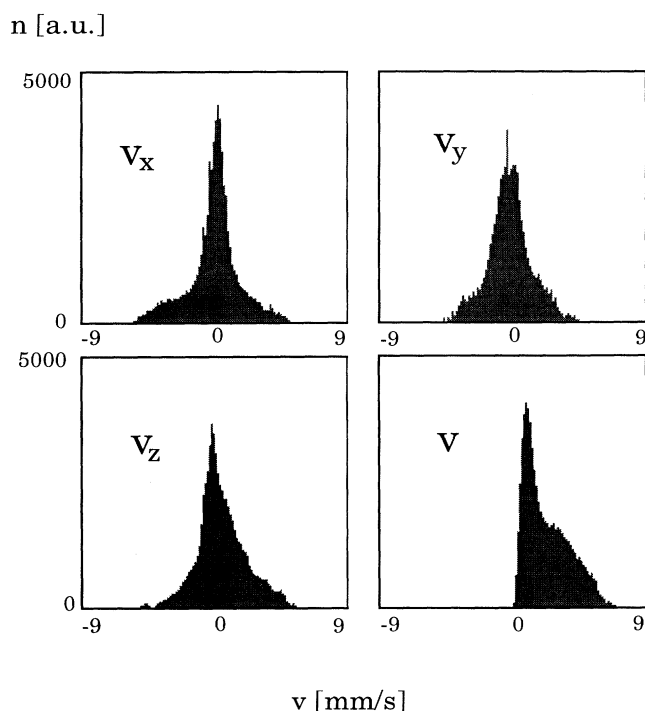
n [a.u.]

v [mm/s]

FIG. 11. Velocity histograms of water flowing through the random-percolation phantom (Fig. 3). The velocity vector field was recorded using the FEVI method (Fig. 1). n is the number of voxels in which the respective velocity component or velocity magnitude was found. The voxel resolution is 250 μm. The resolution of the velocity field is 0.14 mm/s. The main flow direction was along the z axis. The maximum of the velocity magnitude histogram is at 0.8 mm/s.

C. Experiments with the percolation phantom

Figs. 3(a)–3(d) show a comparison of simulated and measured representations of a three-dimensional percolation cluster. Based on the original computer simulated pattern [Fig. 3(a)], a phantom was fabricated, filled with water and imaged using three-dimensional NMR microscopy. The result is a three-dimensional set of spin density data rendered as a gray shade image in Fig. 3(b).

These image data were transferred to a black-white representation [Fig. 3(c)] following the procedure outlined in Sec. V A. Keeping in mind that the mechanical fabrication of the phantom and its NMR examination are unavoidably connected with experimental errors, a relatively good correlation of the pore clusters can be stated already by visual inspection.

The correlation of the simulated and the experimental cluster data was demonstrated quantitatively by evaluating the volume-averaged porosities as a function of the probe-volume radius $\bar{\rho}_V = \bar{\rho}_V(r)$. The result is shown in Fig. 6(c). The characteristic parameters were evaluated as $d_f = 2.53 \pm 0.01$ and $\xi = (4 \pm 1)$ pixel-edge lengths. The fractal dimensionality compares favorably with the values evaluated from the computer-simulated data Fig. 6(a) and 6(b) ($d_f = 2.52 \pm 0.01$ for a matrix $80 \times 80 \times 80$ and $d_f = 2.51 \pm 0.01$ for a matrix $32 \times 32 \times 32$) and predicted by theory ($d_f = 2.53$) [3, 19].

Finally, the percolation backbone was recorded by combining the black-white spin density data Fig. 3(c) with velocity magnitude image data as described in Sec. V B. The result is represented by Fig. 3(d).

The percolation backbone data were again analyzed with respect to the mean volume-averaged porosity as shown in Fig. 6(d). The fractal dimensionality of the backbone was evaluated as $d_f^b = 2.24 \pm 0.01$. This result deviates from the value 1.9 given in [19], but fits well to the range $d_f^b = 2.2$–2.3 found in four independent computer simulations assuming different site occupation probabilities in the range $p - p_c = 0.015$–0.070.

D. Experiments with a natural sponge

Figure 12(a) represents the three-dimensional distribution of static water in a sea sponge as recorded with the aid of three-dimensional spin density imaging. The overall porosity was 0.8.

This image was transferred into black-white contrasts using the procedure described above. The percolation backbone cluster was then derived by combining black-white spin density contrasts with velocity magnitude image data separately recorded with water flowing through the sponge. The result of this "finite-velocity filtering" procedure is represented by percolation backbone image in Fig. 12(b). Figure 9(c) shows the function $\bar{\rho}_V = \bar{\rho}_V(r)$ evaluated from the percolation backbone image data.

The deviation of the characteristic parameters from those derived for random percolation clusters is obvious. The sponge sample evidently does not comply to the self-similarity requirement. Remarkably, the initial radius dependence of the mean volume-averaged poros-
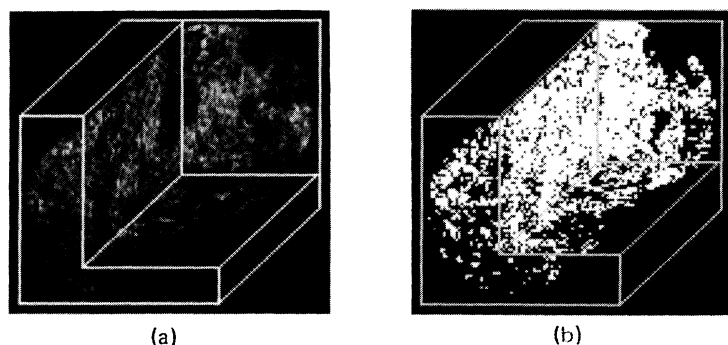
(a)

(b)

FIG. 12. Three-dimensional multisectional representations of NMR image data recorded with a water-filled natural sponge. (a) Spin density image. The voxel matrix and resolution are $80 \times 80 \times 80$ and 100 μm, respectively. (b) Black-white-converted and velocity-filtered spin density of the backbone of (a). Voxels were only taken into consideration if the velocity magnitude in the voxel was ≥ 0.8 mm/s. The resolution of the velocity field recorded with the aid of the FEVI method Fig. 1 was 0.14 mm/s.

ity nevertheless may be represented by a power law as demonstrated in Fig. 9(c).

E. Experiments with glass-bead agglomerates

Tightly packed glass spheres were investigated by imaging water filled into the interstitial space [Fig. 8(b)]. The nominal diameter of the beads was (1.0 ± 0.2) mm. The structure of the agglomerates was less well defined than one might expect from the theoretical point of view [compare the computer drawing of bcc-packed spheres, Fig. 8(a)]. This is due to the unavoidable distribution of the bead diameters and to a certain degree of disorder of the arrangement produced by filling the beads in the sample tube.

The mean volume-averaged porosity as a function of the probe volume radius was evaluated from the black-white-converted spin density image. The result is plotted in Fig. 9(b). Compared with the computer simulated data Fig. 9(a), the oscillatory pattern of the curve is less pronounced, but the slopes of the power-law parts almost coincide.

VI. CONCLUSIONS AND DISCUSSION

In this study we have juxtaposed computer-simulations of percolation clusters to NMR microimaging data of water-filled models fabricated using the computer-simulated patterns as templates. That is a method has been demonstrated permitting us to perform real experiments with any percolation cluster that can be generated on a computer.

The computer simulations are the first for three-dimensional percolation clusters. The numerical results are in accordance with theoretical predictions. A question in this context is in what range of the length scale the potential occurrence of power laws can be recognized safely. In the light of the present study it turned out that at least one to two orders of magnitude must be covered. This finding coincides with a statement by Adler [6].

An evaluation scheme for the experimental data has been developed showing the characteristic laws of the percolation structure. The theoretical predictions have been verified in full detail.

Images of the velocity magnitude of water flowing through percolation clusters unambiguously reveal the structure of the percolation backbone. Here the backbone cluster has experimentally been determined according to the proper physical definition. The method is particularly useful because the percolation backbone is of prominent interest for theoretical as well as for technological considerations.

The experimental and numerical tools developed and tested with the aid of percolation phantoms have been applied to lacunar systems less well characterized from the theoretical point of view. The investigated examples demonstrate that the pore space structures to a certain degree can be characterized formally and in a reasonable range using the same expressions as those developed for fractal percolation clusters. A suitable dependence serving this purpose is the mean volume-averaged porosity as a function of the probe volume radius. In all cases a power-law behavior was found in comparable ranges of the probe volume radius. Lacunar systems of practical importance such as porous rocks, biological objects, building materials, and fabrics therefore can be characterized with a few parameters. Furthermore, images of the velocity magnitude unambiguously reflect the local percolation properties.

Whereas the exponents of the power laws governing the mean volume-averaged porosity relation to the probe volume radius appear to be conspicuously characteristic for the diverse systems of this study, the correlation length is of a less unambiguous nature. First of all, in terms of percolation theory, the correlation length is a function of the net point occupation probability. Furthermore, it can be easily perceived that the sample size plays a role (in the experiments as well as in the computer simulations). Quantitative values therefore can be scarcely predicted in a reliable way. However, from a more practical point of view, the lengths scales inherent to a given lacunar sample can be characterized on this basis.

In this work we have employed NMR microimaging as an experimental tool for the detection of percolation properties. As an alternative NMR method for studies of transport, pulsed-gradient spin-echo techniques should be mentioned. Corresponding investigations of the incoherent flow through a sponge have been performed recently [21]. The results indicate an anomalous behavior indeed. The conclusions that can be drawn on this basis are, however, much less indicative to features specific for percolation. NMR microscopy in the versions employed

in this study is therefore considered to be superior in this respect.

The motivation behind this study arose largely from the wish to have a direct experimental access to transport properties in lacunar systems and to find a suitable formalism for their description. Percolation theory has, however, a wide scope that exceeds that of transport in the literal sense [22]. An example is the recent attempt to delineate fault patterns of earthquake hypocenters [23, 24] on this basis. We believe that the combination of computer simulation and NMR microscopy experiments carried out with lacunar phantoms forms an excellent culture medium for the detailed exploration of the intricacies of percolation phenomena.

[1] *Fractals and Disordered Systems*, edited by A. Bunde and S. Havlin (Springer-Verlag, Berlin, 1991).

[2] R. Orbach, Science **231**, 814 (1986).

[3] A. Kapitulnik, A. Aharony, G. Deutscher, and D. Stauffer, J. Phys. A **16**, L269 (1983).

[4] R. Lenormand and C. Zarcone, Phys. Rev. Lett. **54**, 2226 (1985).

[5] R. Lenormand, G. Daccord, A. Soucemarianadin, E. Touboul, and C. Zarcone, in *Characterization of Porous Solids*, edited by K. K. Unger, J. Rouquerol, K. S. W. Sing and H. Kral (Elsevier, Amsterdam, 1988), Vol. 39.

[6] P.M. Adler, in *Characterization of Porous Solids* (Ref. [5]).

[7] M. D. Rintoul and H. Nakanishi, J. Phys. A. **25**, L945 (1992).

[8] J. Mastorakos and P. Argyrakis, Phys. Rev. E **48**, 4847 (1993).

[9] P. T. Callaghan, *Principles of Nuclear Magnetic Resonance Microscopy* (Clarendon, Oxford, 1991).

[10] M. R. Merrill, Bull. Magn. Reson. **15**, 154 (1993).

[11] G. J. Nesbitt, A. de Groot, T. W. Fens, and J. H. M. Bonnie, Magn. Reson. Imag. **9**, 779 (1991).

[12] O. Lamrous, D. Houi, C. Zarcone, and J. Pradere, Rev. Phys. Appl. **24**, 607 (1989).

[13] M. R. Merrill and Z. Jin, Magn. Reson. Imag. **12**, 345 (1994).

[14] C. N. J. Wagner, J. Non-Cryst. Solids **31**, 1 (1978).

[15] A. S. Clarke and H. Jónsson, Phys. Rev. E **47**, 3975 (1993).

[16] T. W. Redpath, D. G. Morris, R. A. Jones, and J. M. S. Hutchison, Phys. Med. Biol. **29**, 891 (1984).

[17] J. Bittoun, E. Bourroul, O. Jolivet, I. Idy-Peretti, E. Mousseaux, A. Tardivon, and P. Peronneau, Magn. Reson. Med. **29**, 674 (1990).

[18] J. Weis, J. Frollo, and L. Budinski, Z. Naturforsch. Teil A **44**, 1151 (1989).

[19] D. Stauffer and A. Aharony, *Introduction to Percolation Theory* (Taylor and Francis, London, 1985).

[20] A. E. Scheidegger, *The Physics of Flow Through Porous Media* (University of Toronto Press, Toronto, 1974).

[21] F. Klammler and R. Kimmich, Croat. Chem. Acta **65**, 455 (1992).

[22] A. H. Thompson, A. J. Katz, and R. A. Raschke, Phys. Rev. Lett. **58**, 29 (1987).

[23] M. Sahimi, M. C. Robertson, and C. G. Sammis, Physica A **191**, 57 (1992).

[24] M. Sahimi, M. C. Robertson, and C. G. Sammis, Phys. Rev. Lett. **70**, 2186 (1993).
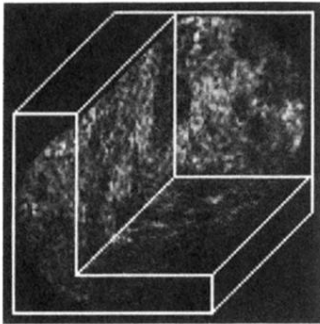
(a)
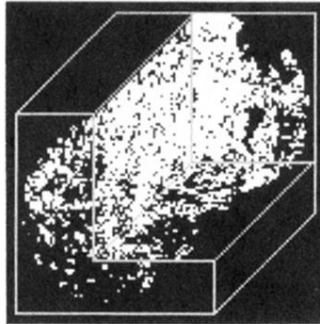
(b)

FIG. 12. Three-dimensional multisectional representations of NMR image data recorded with a water-filled natural sponge. (a) Spin density image. The voxel matrix and resolution are $80 \times 80 \times 80$ and $100 \ \mu$m, respectively. (b) Black-white-converted and velocity-filtered spin density of the backbone of (a). Voxels were only taken into consideration if the velocity magnitude in the voxel was ≥ 0.8 mm/s. The resolution of the velocity field recorded with the aid of the FEVI method Fig. 1 was 0.14 mm/s.
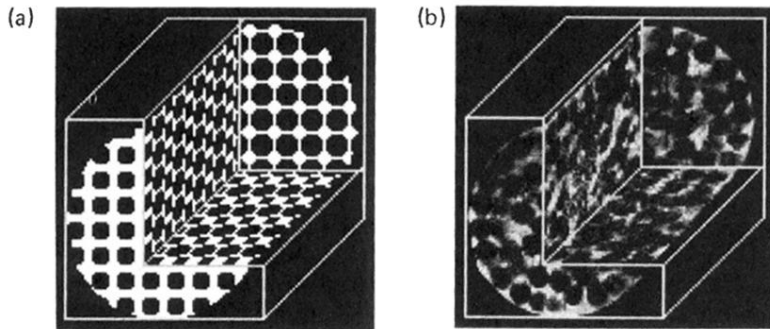
FIG. 8. Three-dimensional multisectional image representations of closely packed spheres. (a) Computer graph of an array of bcc-packed spheres. The same voxel matrix and resolution as in the experiments were assumed, that is, $80 \times 80 \times 80$ and $1/9$ bead diameters, respectively. (b) Experimental spin density image of water filled in the interstitial space of a glass-bead agglomerate. The bead diameter was (1.0 ± 0.2) mm. The voxel resolution was 100 μm.